Implications of Ground Motion Data Recorded in the M7.6 Chi-Chi, Taiwan Earthquake of September 21, 1999

Yi-Ben Tsai.
Institute of Geophysics, National Central University, Chung-Li, Taiwan

ABSTRACT

A disastrous earthquake took place in central Taiwan at 01:47 of September 21, 1999 (Taiwan local time). The Seismology Center of the Central Weather Bureau (CWB) located the epicenter near the town of Chichi, Nantou County . The magnitude of this earthquake was M_L 7.3 (CWB) and M_W 7.6 (NEIC). The earthquake has caused heavy casualties and building damages: 2,539 people killed or missing, 11,306 people injured; 51,751 household units totally collapsed, 54,406 household units partially collapsed. In addition, there were widespread destruction and disruption of lifelines, including roads and bridges, water supply, gas supply, communication and electricity. The Chi-Chi, Taiwan earthquake produced a rich set of 441 strong ground motion recordings. In this paper we present some results from analysis of these recordings.

First, we found that the overall level of the observed horizontal peak ground acceleration (PGA) values was relatively low (about 50% less) when compared with what would be predicted for an earthquake of the same magnitude by existing attenuation models based on worldwide data. High horizontal PGA values at sites on the hanging wall and within 20 km of the surface fault ruptures are notable exceptions. The horizontal PGA values are indistinguishable among the four different site classes. However, the horizontal PGA values in Taipei Basin, Ilan Plain, and Hwalien areas are significantly higher than the average at similar distances. Unlike the horizontal PGA, the observed horizontal peak ground velocity (PGV) values are relatively high (at least 100% higher) when compared with what would be predicted for an earthquake of the same magnitude by an existing PGV attenuation model based on worldwide data. Thus, as far as peak ground motion parameters are concerned, the Chi-Chi earthquake may be called a high-PGV, low-PGA earthquake.

Next, we analyzed the 5% damped acceleration response spectrum shapes for the four different site classes B, C, D, and E, in order to study possible dependence of the response spectrum shape on local site conditions. It is found that the peak spectral amplification factor ranges between 2.3 and 2.5 for all four classes of site conditions. In general, the response spectrum shape for Class B sites on soft rocks older than the Pliocene age has spectral amplification for periods up to about 1.5 seconds. The spectral amplification of Classes C and D sites on stiff soils occurs over periods up to about 2.0 seconds. The spectral amplification of Class E sites on soft soils occurs over periods up to about 3.0 seconds. The response spectrum shapes for Taipei Basin and Ilan Plain are quite similar to Class E sites, whereas Hwalien area is similar to Class C or D sites.

Finally, we analyzed the observed characteristics of acceleration response spectra from 44 near-fault sites. For the eight sites within 2 km from the surface fault ruptures, the median horizontal PGA value is about 0.5 g. The corresponding spectral peak is about 1.0 g. The median-plus-one-standard-deviation horizontal PGA value is about 0.7 g and the corresponding spectral peak is

about 1.8 g. Thus, for sites within 2 km from the surface fault ruptures, application of a scaling factor of 1.5 to the current seismic design spectrum anchored at a PGA value of 0.33 g for Zone 1A appears to be appropriate. For the 18 sites located at 2 to 10 km from the surface fault ruptures, the median horizontal PGA value is about 0.25 g. The corresponding peak spectral value is about 0.6 g. The median-plus-one-standard-deviation horizontal PGA value is about 0.4 g and the corresponding peak spectral value is about 0.8 g. Thus, for sites between 2 and 10 km from the surface fault ruptures, the current seismic design spectrum anchored at a PGA value of 0.33 g for Zone 1A appears to be adequate. For the 33 sites at 10 to 20 km from the surface fault ruptures, the median horizontal PGA value is about 0.18 g and the corresponding peak spectral value is about 0.45 g. The median-plus-one-standard-deviation horizontal PGA value is about 0.3 g and the corresponding peak spectral value is about 0.7 g. Thus, for sites located between 10 and 20 km from the surface fault ruptures, the current seismic design spectrum anchored at a PGA value of 0.33 g for Zone 1A is more than adequate.

Introduction

On September 21, 1999 at 1:47 Taiwan local time (September 20, 17:47 GMT), the central Taiwan area was hit by a disastrous earthquake of M_L magnitude 7.3 (the Seismology Center of the Central Weather Bureau (CWB). The Mw magnitude of the earthquake was 7.6 (NEIC). The epicenter of the event was located at 120.82^oE, 23.85^oN. The focal depth was about 8 km (Shin et al., 2000). This was the largest earthquake to strike central Taiwan in this century.

This earthquake was caused by sudden rupture of the Chehlungpu fault. Both the unusually large surface fault displacements and the very strong ground shakings caused enormous destruction. The most severely devastated areas were in Nantou and Taichung Counties as well as Taichung City in central Taiwan. The most strongly shaken area has about 1.2 million residents. It also caused significant casualties and damages in other cities and counties both in central and northern Taiwan. According to latest official reports, a total of 2,489 people were killed, 11,306 injured, 51,751 household units totally collapsed, 54,406 houldhold units partially collapsed. There were 50 people still missing. This was the second most disastrous earthquake in Taiwan history, after the April 21,1935 earthquake of M_L 7.1 which occurred just north of the Chi-Chi earthquake and killed 3,276 people in Taichung and Miaoli counties.

Values Of Rapid Earthquake Information

At 102 seconds after the earthquake, the Taiwan Rapid Earthquake Information Release System (TREIRS) operated by the Seismology Center of the Central Weather Bureau recorded and located automatically the time, location magnitude of the earthquake. The information provided to the public also included recorded intensity data at many locations throughout Taiwan (Wu et al., 1998, 1999). The availability of rapid and reliable earthquake information was instrumental to the formation of the National Emergency Operation Center immediately to mobilize and deploy search-and-rescue personnel and relief materials to the impacted areas even in the middle of the night.

Figure 1 shows the locations of seismic stations in the Taiwan Rapid Earthquake Information Release System. Figure 2 shows the target times, modes, and intended recipients of rapid

earthquake information. It aimed to have intensity information available in one minute, location and magnitude information available in three minutes. The information is disseminated by Pager, e-mail, fax, internet and ftp. The information is sent to the Central Fire Administration, City and County Fire departments, other government agencies and officials, and news media. Figure 3 shows the actual CWB earthquake report for the Chi-Chi earthquake. The system was also extremely valuable in providing rapid and reliable information about strong aftershocks and earthquakes in other areas in the days following the Chi-Chi earthquake. The people, both inside and outside the disaster areas, were very frightened by then. Timely and reliable earthquake information greatly helped to calm people and to prevent rumors.

Surface Ruptures Of The Causative Chehlungpu Fault

By dawn in the morning immediately following the earthquake, many geologists rushed to the epicenter areas to make reconnaissance surveys of possible surface fault ruptures. It was soon discovered that the Chehlungpu fault was the culprit of the earthquake. It slipped almost continuously, although sinuously, along its whole length extending southward from Fengyuan in the northern end to Tongtou in the southern end. Soon later, splays of NE-trending surface fault ruptures were found extending northeastward from Fengyuan toward Shihkang. Total length of the surface fault ruptures was estimated at about 100 km (Central Geological Survey, 1999). Figure 4 shows the location of the Chehlungpu fault and the amount of slips along the fault. Photos 1 to 4 show destruction of some structures caused by the fault ruptures. The structures destroyed included a dam (photo 1), bridges (photo 2), schools (photo 3), houses (photo 4), etc.

Both uplift and left-lateral strike-slip displacements were observed at most outcrop locations. It is clear that the Chehlungpu fault was an oblique thrust fault. This was consistent with the fault-plane solution obtained by the first motion polarities and moment tensor inversions as shown in Figure 4. It is remarkable that the amount of slips increased persistently from a little over one meter in the southern end and to almost ten meters observed near the northern end of the fault. Figure 5 shows the regional geology of the surrounding areas (Lee et al., 1999). The Chehlungpu fault clearly marks the boundary between the Pliocene and Quaternary formations. An E-W section across the fault at the bottom of the figure shows a series of imbricated thrust faults dipping to the east. The Chehlungpu fault is just one of them. Figure 4 also shows the locations of background seismicity and strong aftershocks of the Chi- Chi earthquake. It is seen that most aftershocks took place far away from the Chehlungpu fault in the zones of active background seismicity east of the Chelnungpu fault. The zones of active background seismicity appeared to define the boundaries of the displaced crustal block. Figure 4 additionally shows the velocity waveforms of the E-W component integrated from original acceleration records at seven stations happened to align along the fault trace. It is seen from the differential timings among the big pulses that the fault rupture started from the hypocenter first and then propagated toward the north and south. The rupture velocity can be estimated at about 2 km/sec. The big pulse near the northern end was significantly enhanced due to rupture directivity.

The Chehlungpu fault was a product of plate collision in Taiwan area. Figure 6 shows the configurations of the Philippine Sea plate and the Eurasian plate in Taiwan area. It is seen from the figure that the two plates collide with each other along the Taitung Longitudinal Valley. The Philippine Sea plate subducts northward under the Eurasian plate in northeastern Taiwan. In the

meantime, The Eurasian plate is subducting eastward under the Philippine Sea plate in southeastern Taiwan.

Figure 7 shows the GPS measurement results on the velocity of crustal movement in Taiwan (Yu et al., 1997). The Philippine Sea plate is seen to move northwestward toward Taiwan at a velocity of more than 8 cm/year. It is noted that the crustal velocity decreases progressively westward, causing compression across most of the island of Taiwan and resulted in series of imbricated faults, as shown previously in Figure 5.

Strong Ground Motion Peak Values And Permanent Displacements

The Chi-Chi earthquake was well recorded by 441 high-quality free-field strong-motion accelerographs. Figure 8 shows the locations of these recording instruments at different geologic site conditions. The recording sites were classified into four classes, namely B, C, D, and E, according to geologic age (Lee, et al., 2001). Figure 9 shows distributions of the recorded horizontal peak ground acceleration (PGA) values along with the total fatalities of each county or city. It can be seen that the PGA values are significantly higher at sites along the Chehlungpu fault and in the areas to the east of the fault than other areas. This was due to its thrust faulting mechanism that often caused stronger ground motions on the hanging wall block (Abrahamson and Somerville, 1996). This ground motion feature was closely correlated with the distribution of fatality rates in the meizoseismal area, as shown in Figure 10 below.

Figure 10 shows the total fatalities and fatality rates in individual townships, as well as the seismic intensity distribution in the near-fault areas in central Taiwan. It is apparent that all large fatalities took place in the towns experiencing seismic intensity greater than 250 gals. This pattern becomes even clearer when we look at the distribution of the fatality rate. We use the necessary population data from the demographic summary for 1999 (National Office of Statistics, 2000b). The fatality rates in towns experiencing more than 400 gals ranged from 0.054% to 1.112%, whereas the fatality rates were all below 0.002% in towns experiencing less than 250 gals. The only notable exception in this lower intensity zone was the town of Yuanlin in Changhua County where a fatality rate of 0.019% occurred. It was found that severe liquefaction had caused collapse of many buildings in this town (National Center for Research in Earthquake Engineering, 1999).

Figure 11 shows the plot of horizontal PGA values as function of the closest distance to the seismogenic zone, according to Campbell's definition (Campbell, 1997). The data points are plotted according to the four site classes. In addition, the data points from the Taipei Basin, Ilan Plain, and Hwalien areas are plotted separately. In the figure we also plot the Campbell's median and median +/- one standard deviation PGA curves for M_W 7.6 that are modified by multiplying a factor of 0.55 to fit the data points. From the figure we can see the slope of Campbell's curve fit quite well with the data points from the Chi-Chi earthquake. However, the Campbell's curves would significantly overestimate relative to the actual PGA values. It is noted that the PGA values from the Taipei Basin, Ilan Plain, and Hwalien area are significantly higher than the rest of the data set. This was probably due to the basin amplification effects.

Figure 12 shows the integrated horizontal peak ground velocity (PGV) values in cm/sec. It can

be seen that the PGV values are significantly higher at sites along the Chehlungpu fault and in the areas to the east than in other areas. This was again due to its thrust faulting mechanism that often caused stronger ground motions on the hanging wall block.

Figure 13 shows the plot of horizontal PGV values as function of the closest distance to the seismogenic zone, according to Campbell's definition (Campbell, 1997). The data points are plotted according to the four site classes. In addition, the data points from the Taipei Basin, Ilan Plain, and Hwalien areas are plotted separately. In the figure we also plot the Campbell's median and median +/- one standard deviation PGV curves for M_W 7.6 that are modified by multiplying a factor of 2.18 to fit the data points. From the figure we can see the slope of Campbell's curve fit quite well with the actual data points from the Chi-Chi earthquake. However, the Campbell's curves would significantly underestimate relative to the actual PGV values. It is noted that the PGV values from the Taipei Basin, Ilan Plain, and Hwalien areas are significantly higher than the rest of the data set. This was probably due to basin amplification effects.

Figure 14 shows the distribution of integrated horizontal permanent displacement (PD) in meters. In the figure we also show the displacement values measured by GPS (Yu, 1999). It is found that the two sets of measurements are highly consistent with each other. This is the first time that permanent co-seismic ground displacements were observed by so many accelerographs. From the figure we can see very clearly the horizontal displacement vectors of the hanging wall block rotate clockwise in direction from south to north and increase in magnitude from about 2 meters in the south to almost 10 meters in the north. These displacement vectors are also consistent with the dislocations observed from the surface fault ruptures. Figure 15 shows the original accelerograms and the integrated velocity and displacement waveforms observed at the Shihgang station (TCU068). The records indicate the fault displaced smoothly and quickly near its northern end.

Figure 16 shows the first-order estimation of the dip-slip and strike-slip displacements in the southern, central and northern segments of the Chelungpu fault. Figure 17 compares the observed and calculated horizontal and vertical displacements across the southern, central and northern segments of the fault. The fittings are reasonably close.

Dependence Of Response Spectrum Shape On Local Site Conditions

In the following we analyzed the 5% damped acceleration response spectrum shapes for four different site classes B, C, D, and E in order to study possible dependence of response spectrum shape on local site conditions. For the sake of easy comparison, we use four modified seismic design spectrum shapes for soil Types 1,2,3 and Taipei Basin sites, respectively. They are obtained by replacing the constant value of 1.0 at long periods (T) on current seismic design spectra in the Taiwan Building Code (TBC) with a 1/T function. In addition, the amplification factor is increased from 2.0 to 2.5 for the modified design spectrum for Taipei Basin in current Taiwan Building Code (TBC).

Figure 18 shows the normalized response spectrum shape for Class B sites on rocks of Miocene age or older, as well as the four modified seismic design spectrum shapes. The observed median curve has spectral amplification over periods up to about 1.5 seconds. It is similar to the

modified seismic design spectrum for Type 2 sites in the current Taiwan Building Code (TBC). For periods greater than 1 second the observed median curve is clearly below the modified TBC spectrum level. The peak spectral amplification factor is about 2.3.

Figure 19 shows the normalized response spectrum shape for Class C sites on soft rocks of Pliocene or early Pleistocene ages, as well as the four modified seismic design spectrum shapes. The observed median curve has spectral amplification over periods up to about 2.0 seconds. It is similar to the modified seismic design spectrum for Type 3 sites in the current Taiwan Building Code (TBC). For periods shorter than 5 seconds the observed median curve follows closely with the modified Type 3 spectrum. The peak spectral amplification factor is about 2.4.

Figure 20 shows the normalized response spectrum shape for Class D sites on stiff soils of late Pleistocene age or younger, as well as the four modified seismic design spectrum shapes. The observed median curve has spectral amplification over periods up to about 1.7 seconds. It is similar to the modified seismic design spectrum for Type 3 sites in the current Taiwan Building Code (TBC). For periods greater than 1.5 seconds the observed median curve is clearly below the modified TBC Type 3 spectrum level. The peak spectral amplification factor is about 2.3.

Figure 21 shows the normalized response spectrum shape for Class E sites on soft soils of Holocene age or younger, as well as the four modified seismic design spectrum shapes. The observed median curve has spectral amplification over periods up to about 3.0 seconds. It follows closely but falls slightly below the modified seismic design spectrum for Taipei Basin sites in the current Taiwan Building Code (TBC). For periods greater than 4.0 seconds the observed median curve deviates more below the modified TBC Taipei Basin spectrum level. The peak spectral amplification factor is about 2.4.

In summary, we have seen clear dependence of the response spectrum shape on local site conditions from the recordings of the Chi-Chi earthquake. The median spectrum shape of Class B sites is similar to the modified Type 2 seismic design spectrum in current TBC. The median spectrum shapes of Classes C and D sites are similar to the modified Type 3 seismic design spectrum in current TBC. Finally, the median spectrum shape of Class E sites is similar to the modified Taipei Basin seismic design spectrum in current TBC.

Near-Fault Ground Acceleration Response Spectra

Finally, we analyzed the observed acceleration response spectra from 64 near-fault sites to study their characteristics. Figure 22 shows the response spectra for the 9 sites within 2 km from the surface fault ruptures. The observed median response spectrum has a horizontal PGA value of about 0.5 g and a corresponding spectral peak of about 1.0 g. The median-plus-one-standard-deviation horizontal PGA value is about 0.7 g and the corresponding spectral peak is about 1.8 g. In the figure are shown the three modified TBC seismic design spectra anchored at a PGA of 0.33 g. It is found that the observed median curve for sites located within 2 km of the surface fault ruptures matches well with the Type 3 design spectrum, except at very short periods. After multiplied by a scaling factor of 1.5, the modified Type 3 seismic design spectrum anchored at a PGA value of 0.33 g for Zone 1A will almost match the median-plus-one-standard-deviation curve, as shown in Figure 23.

Figure 24 shows the response spectra for the 21 sites located at 2 to 10 km from the surface fault ruptures. The median horizontal PGA value is about 0.25 g. The corresponding peak spectral value is about 0.6 g. The median-plus-one-standard-deviation horizontal PGA value is about 0.4 g and the corresponding peak spectral value is about 0.8 g. Thus, for sites located between 2 and 10 km from the surface fault ruptures the current seismic design spectrum anchored at a PGA value of 0.33 g for Zone 1A would be more than adequate.

Figure 25 shows the response spectra for the 34 sites located at 10 to 20 km from the surface fault ruptures. The median horizontal PGA value is about 0.18 g with a corresponding peak spectral value of about 0.45 g. The median-plus-one-standard-deviation horizontal PGA value is about 0.3 g with a corresponding peak spectral value of about 0.7 g. Thus, for sites located between 10 and 20 km from the surface fault ruptures the current seismic design spectrum anchored at a PGA value of 0.33 g for Zone 1A would be much more than adequate.

Acknowledgements

References

Abrahamson, N.A. and Somerville, P.G. (1996). Effects of the hanging wall and footwall on ground motions recorded during the Northridge Earthquake, Bull. Seism. Soc. Am.,86, S93-S99.

Campbell, Kenneth W.(1997). Attenuation relationships for shallow crustal earthquakes based on California strong motion data, Seism. Research Letters, 180-189.

Campbell, K. W.(1997). Empirical near-source attenuation relationships for horizontal and vertical components of peak ground acceleration, peak ground velocity, and pseudo-absolute acceleration response spectra, Seism. Res. Letter, 68, 154-179.

Central Geological Survey (1999). Report on geological investigations of the 921 earthquake (in Chinese), 315 pp.

Chang, C. H., Y. M. Wu, T. C. Shin, and C. Y. Wang (2000). Relocation of the 1999 Chi-Chi earthquake in Taiwan, TAO (Terrestrial, Atmospheric and Oceanic Sciences), vol. 11, no. 3, 581-590.

Institute of Building Research (1999). Preliminary report on surveys of damaged buildings from the great 921 Chi-Chi earthquake (in Chinese), 178 pp.

Lee, W. H. K., T. C. Shin, K. W. Kuo, and, K. C. Chen (1999). CWB free-field strong-motion data from the 921 Chi-Chi earthquake, Volume 1: Digital acceleration files on CD-Rom,

Seismology Center, Central Weather Bureau, Taipei, Taiwan.

Liu, Kun-Sung, Shin, Tzay-Chyn and Tsai, Yi-Ben (1999). A free-field strong motion network in Taiwan: TSMIP, TAO, 10, 377-396.

Ma, K. F., C. T. Lee, Y. B. Tsai, T. C. Shin, and, J. Mori (1999). The Chi-Chi, Taiwan earthquake: Large surface displacements on inland thrust fault, EOS, v.80, 605-611.

Shin, T.C., K.W. Kuo, W.H.K. Lee, T.L. Teng, and Y.B. Tsai (1999). A preliminary report on the 1999 Chi-Chi (Taiwan) earthquake, Seism. Res. Lett., submitted.

Shin, T. C. (2000). Some seismological aspects of the 1999 Chi-Chi earthquake in Taiwan, TAO (Terrestrial, Atmospheric and Oceanic Sciences), vol.11, no.3, 555-566.

Tsai, Y. B. and M. W. Huang (2000). Strong ground motion characteristics of the Chi-Chi, Taiwan earthquake of September 21, 1999, Earthquake Engineering and Engineering Seismology, vol.2, no.1, 1-21.

Wu, Y. M., T. C. Shin, and Y. B. Tsai (1998). Quick and reliable determination of magnitude for seismic early warning, Bull. Seism. Soc. Am. Vol. 88, No5, 1254-1259.

Yih-Min Wu, Jen-Kuang Chung, Tzay-Chyn Shin, Yi-Ben Tsai, William H. K. Lee (1999). Development of seismic rapid reporting and early warning system in Taiwan, IUGG99 abstracts, A6 or A126.

Wu, Y. M., W. H. K. Lee, C. C. Chen, T. C. Shin, T. L. Teng, and Y. B. Tsai (2000). Performance of the Taiwan rapid earthquake information release system (RTD) during the 1999 Chi-Chi (Taiwan) earthquake, Seism. Res. Let., 71, 338-343.

Yu, S.B., Chen, H.Y. and Kuo, L.C. (1997). Velocity field of GPS stations in the Taiwan area, Tectonophysics 274, 41-59.
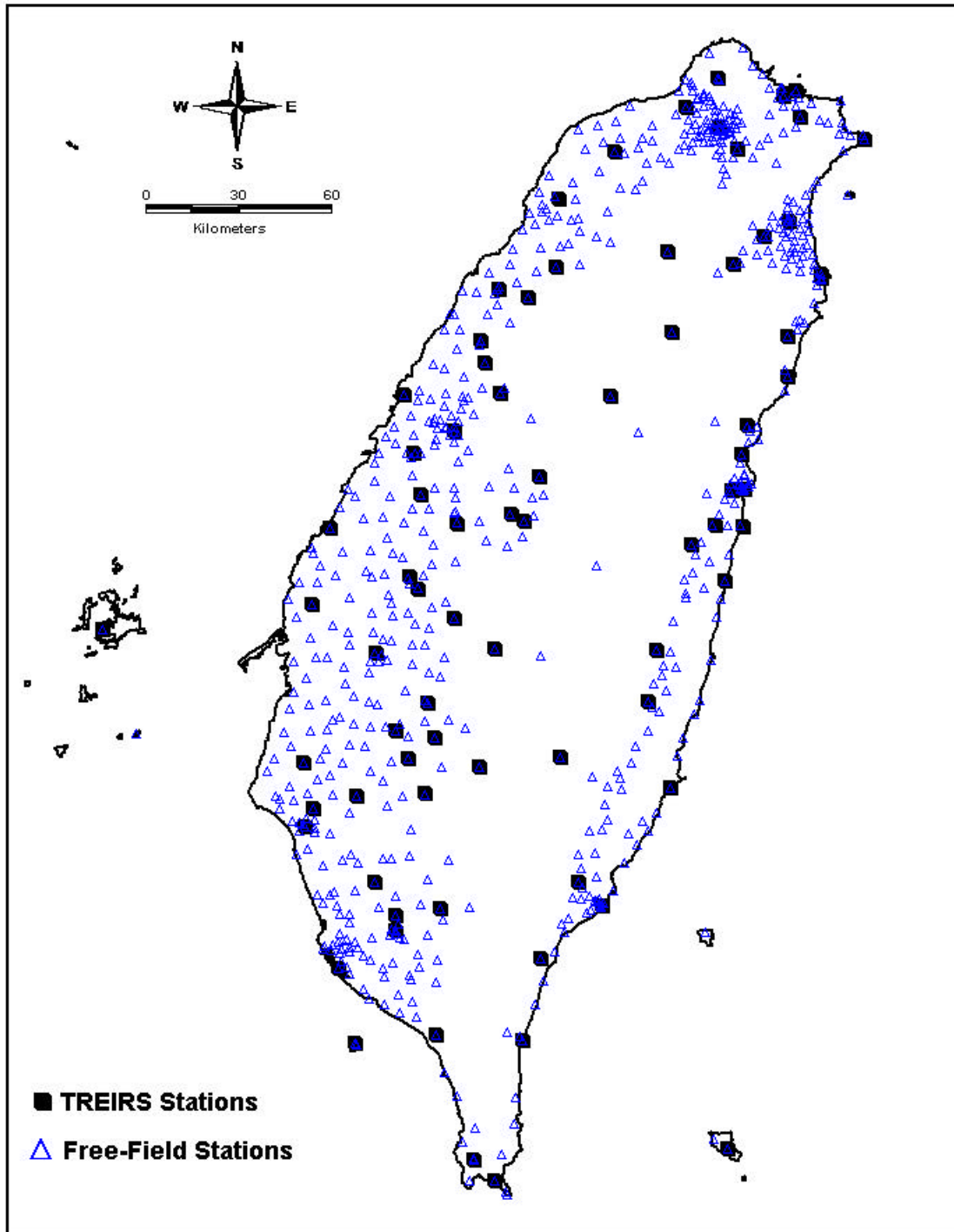
Figure 1.   Locations of seismic stations for the Taiwan Rapid Earthquake Information System and the free-field strong motion network.
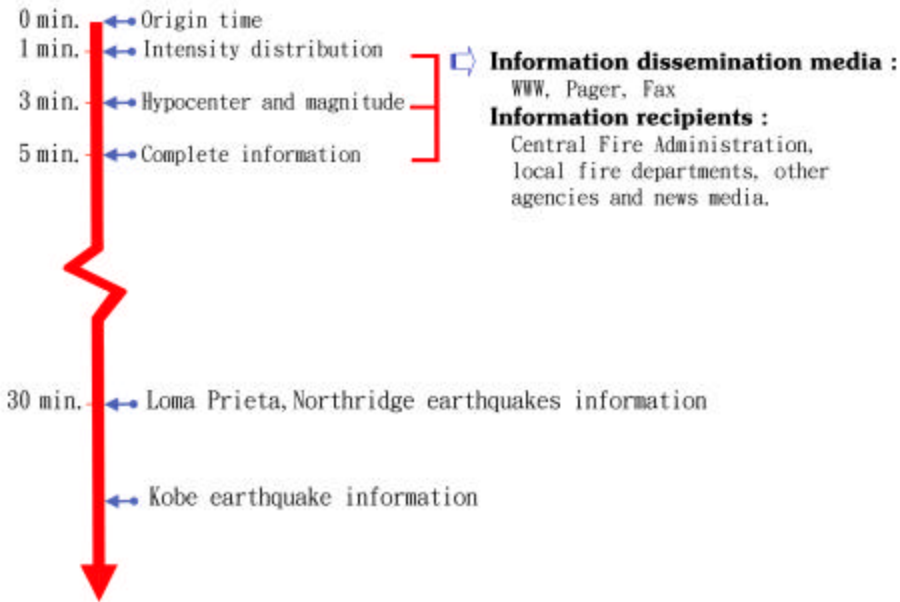
Figure 2.   Target time schedule of Taiwan rapid Earthquake Information System
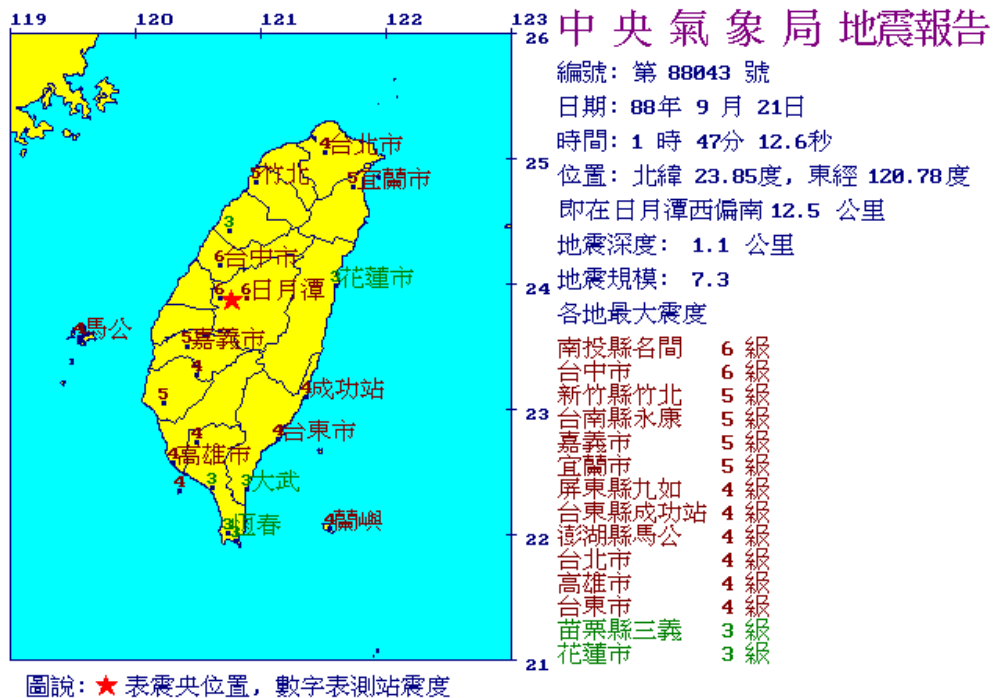
Figure 3.   The Central Weather Bureau's Earthquake No.88043 on the Chi-Chi earthquake of September 21, 1999.
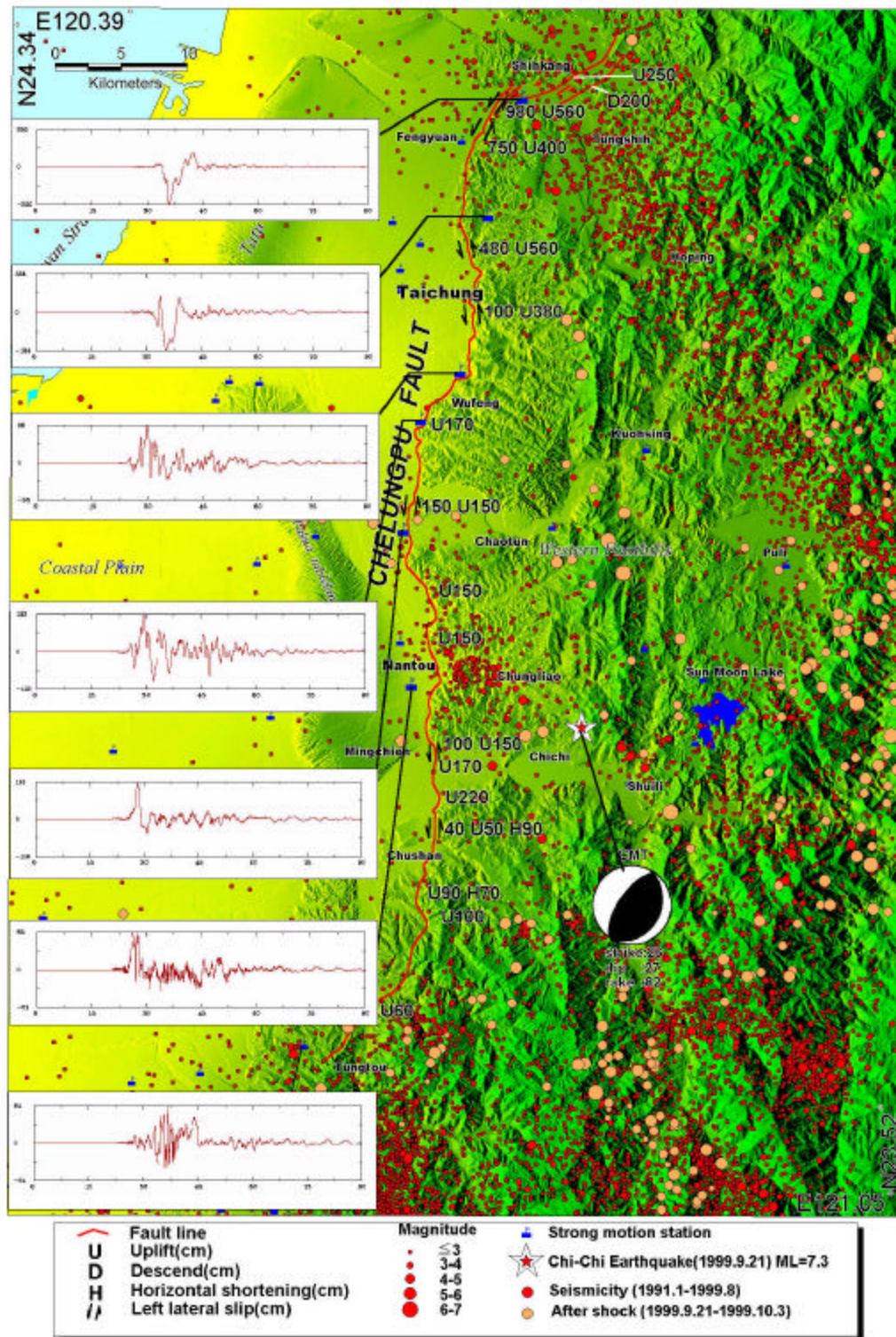
Figure 4.   The Chehlungpu fault, and the epicenter of the Chi-Chi earthquake. Also shown are background seismicity (in red dots), strong aftershocks(orange dots), E-W component velocity waveforms along the fault line.
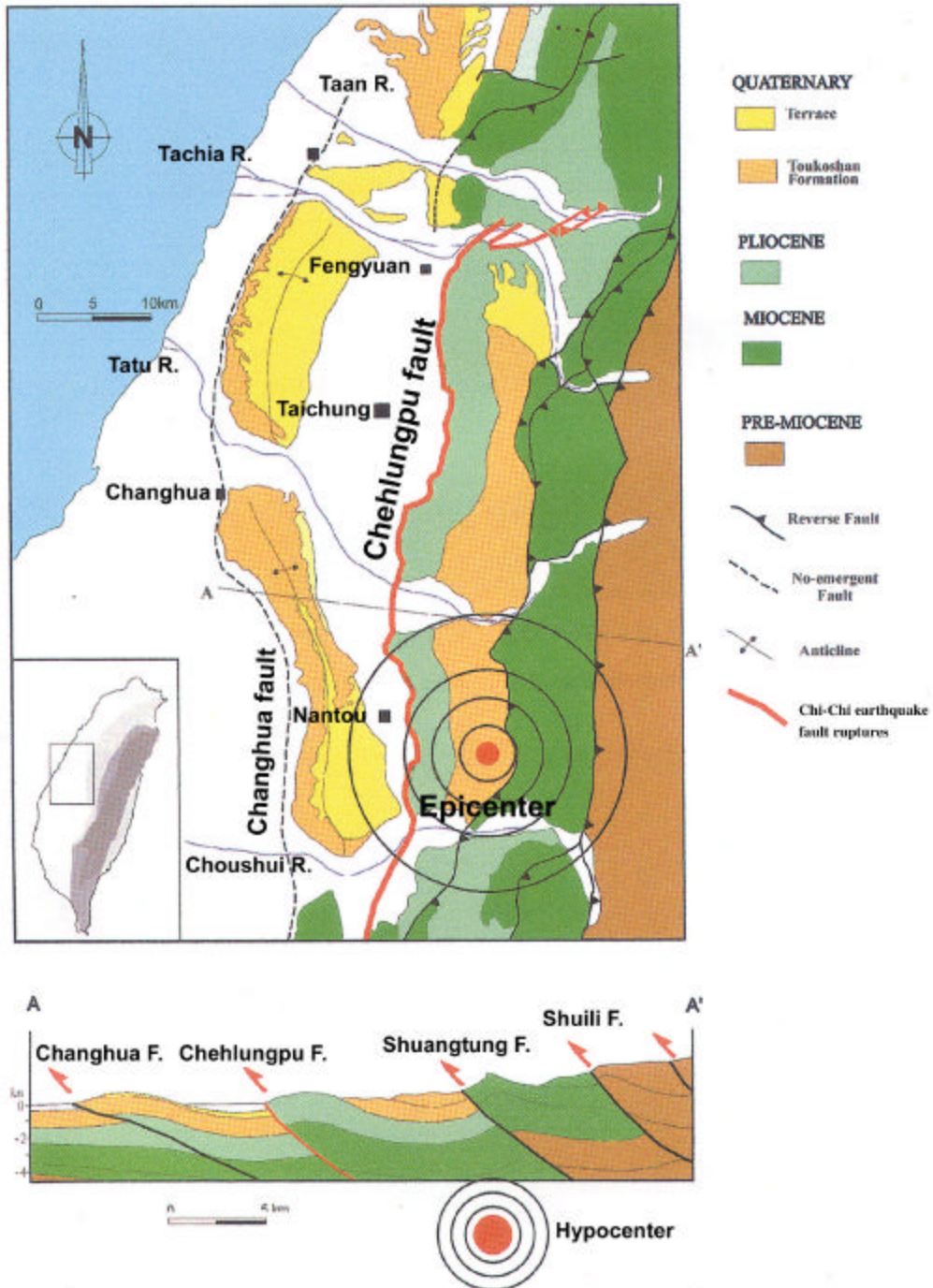
Geologic map and cross-section of central Taiwan and location of the Chi-Chi earthquake

Figure 5.   Regional geology surrounding the Chehlungpu fault and an E-W cross section.(After Lee et al, 1999)
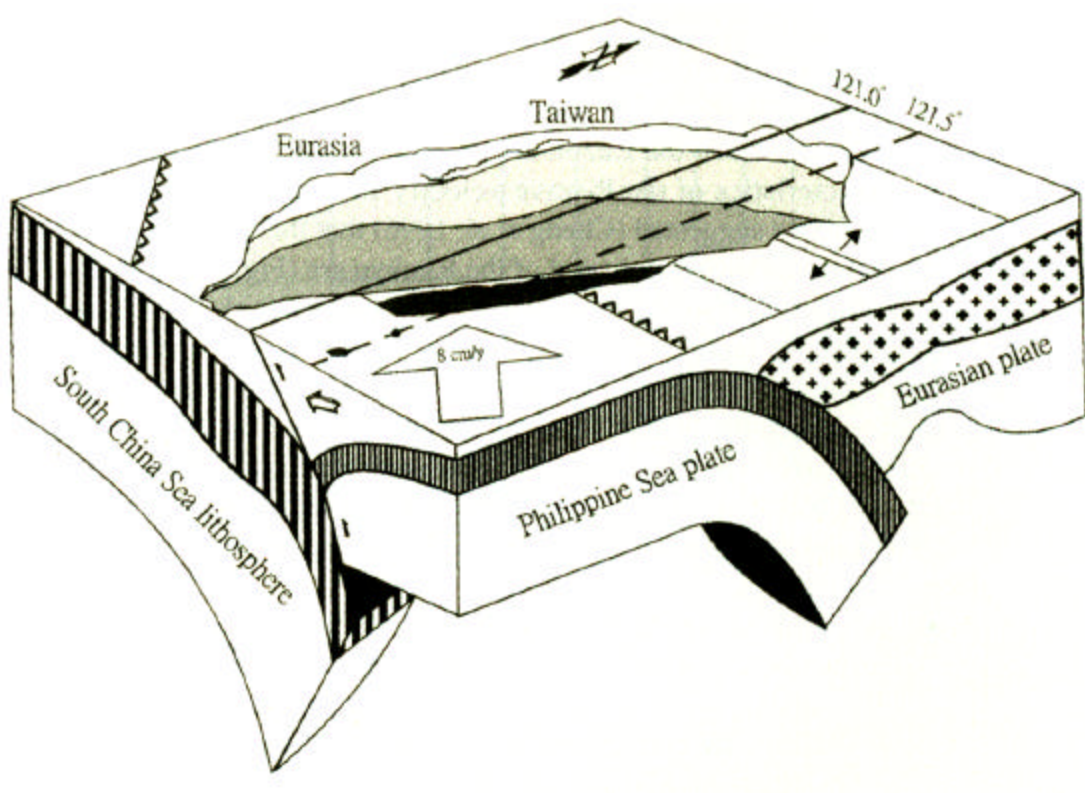
Figure 6. Plate configurations in Taiwan area (after Angelier, 1986).
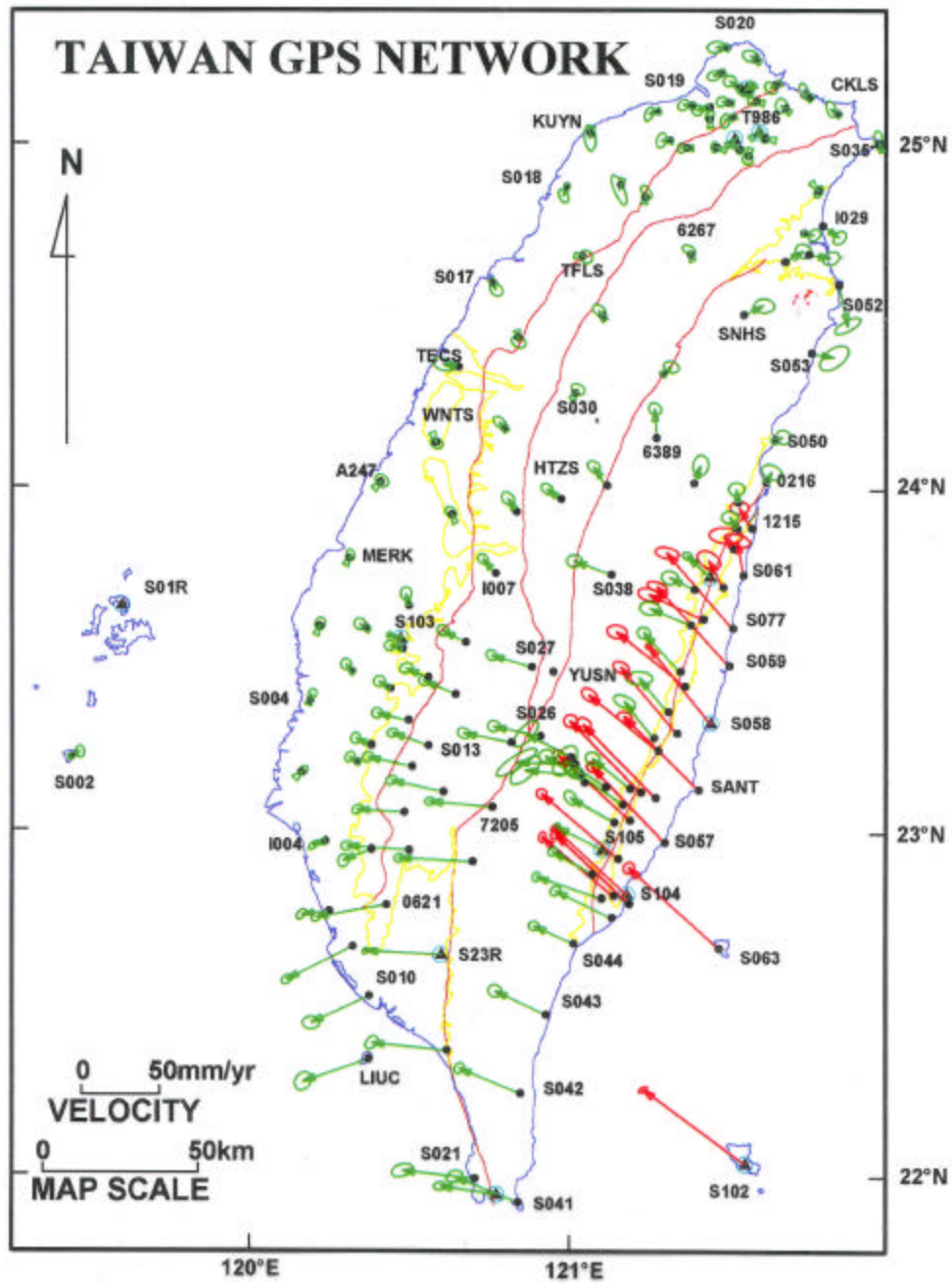
Figure 7.   The velocity field of crustal movement measured by GPS (after Yu et al., 1997).
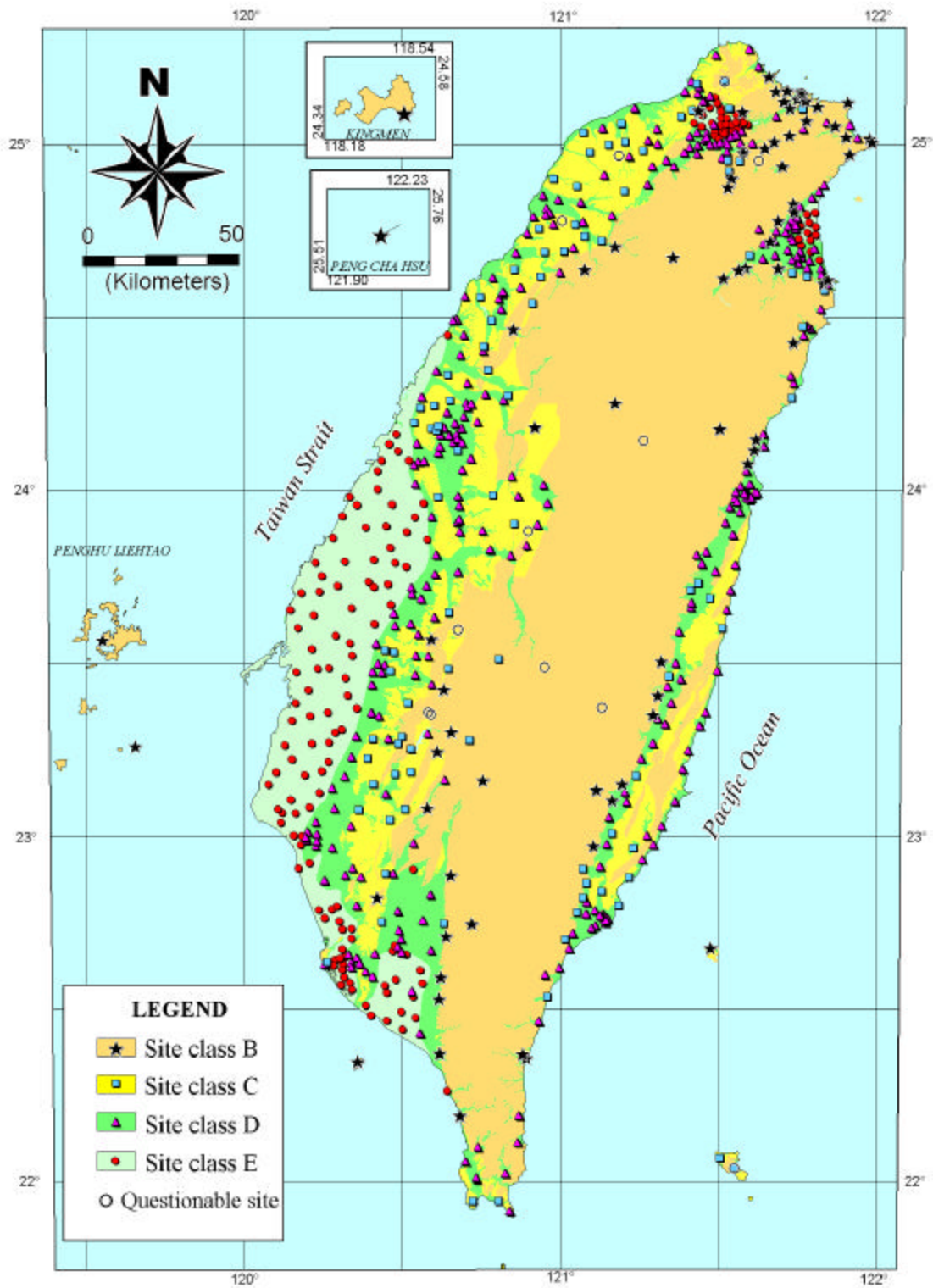
Figure 8.   Free-field strong motion accelerograph sites and geologic conditions of Taiwan (Lee et al., 2001).
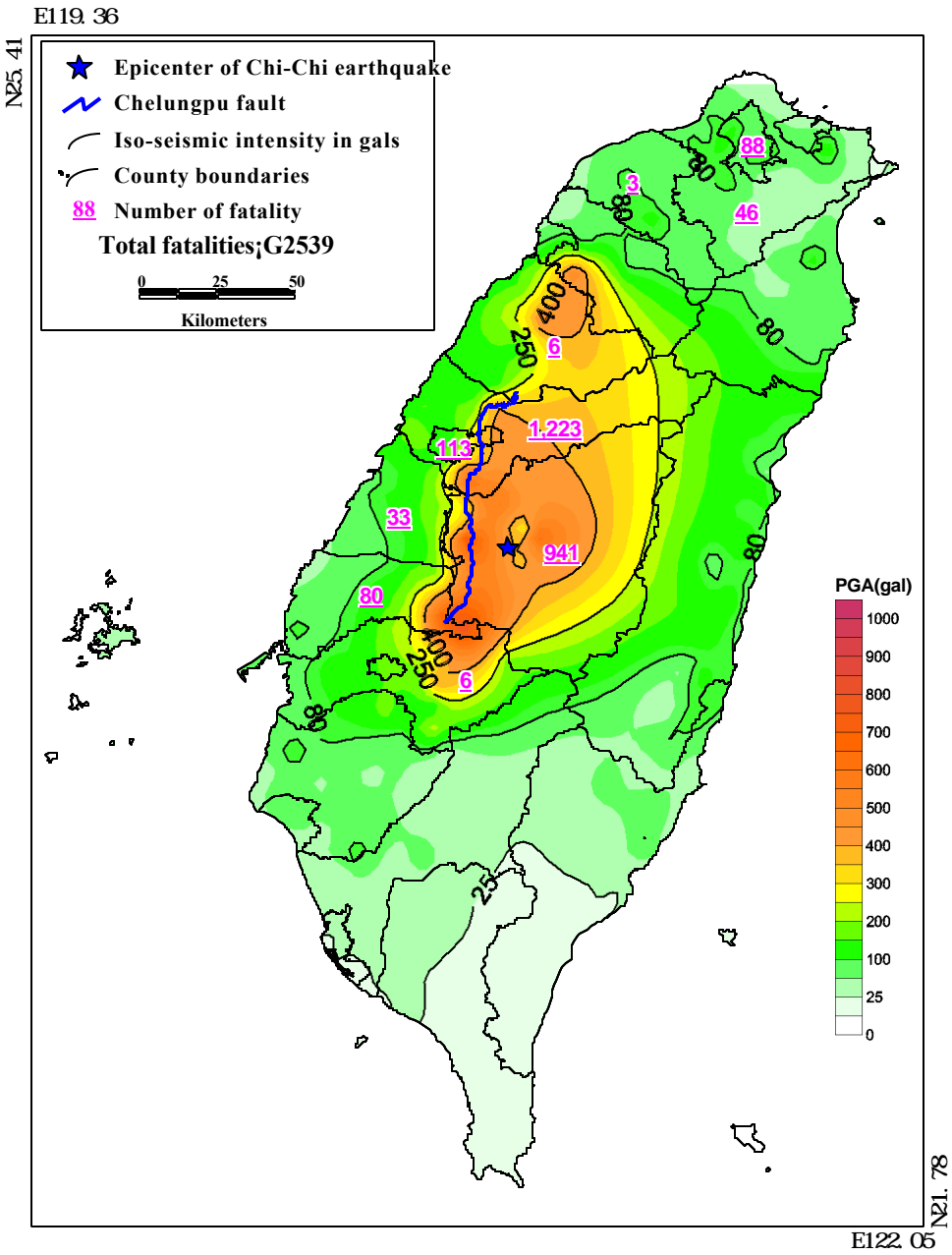
Figure 9.   Contours of horizontal peak ground acceleration in gals and the total number of fatality in each county or city due to the Chi-Chi, Taiwan earthquake of September 21, 1999
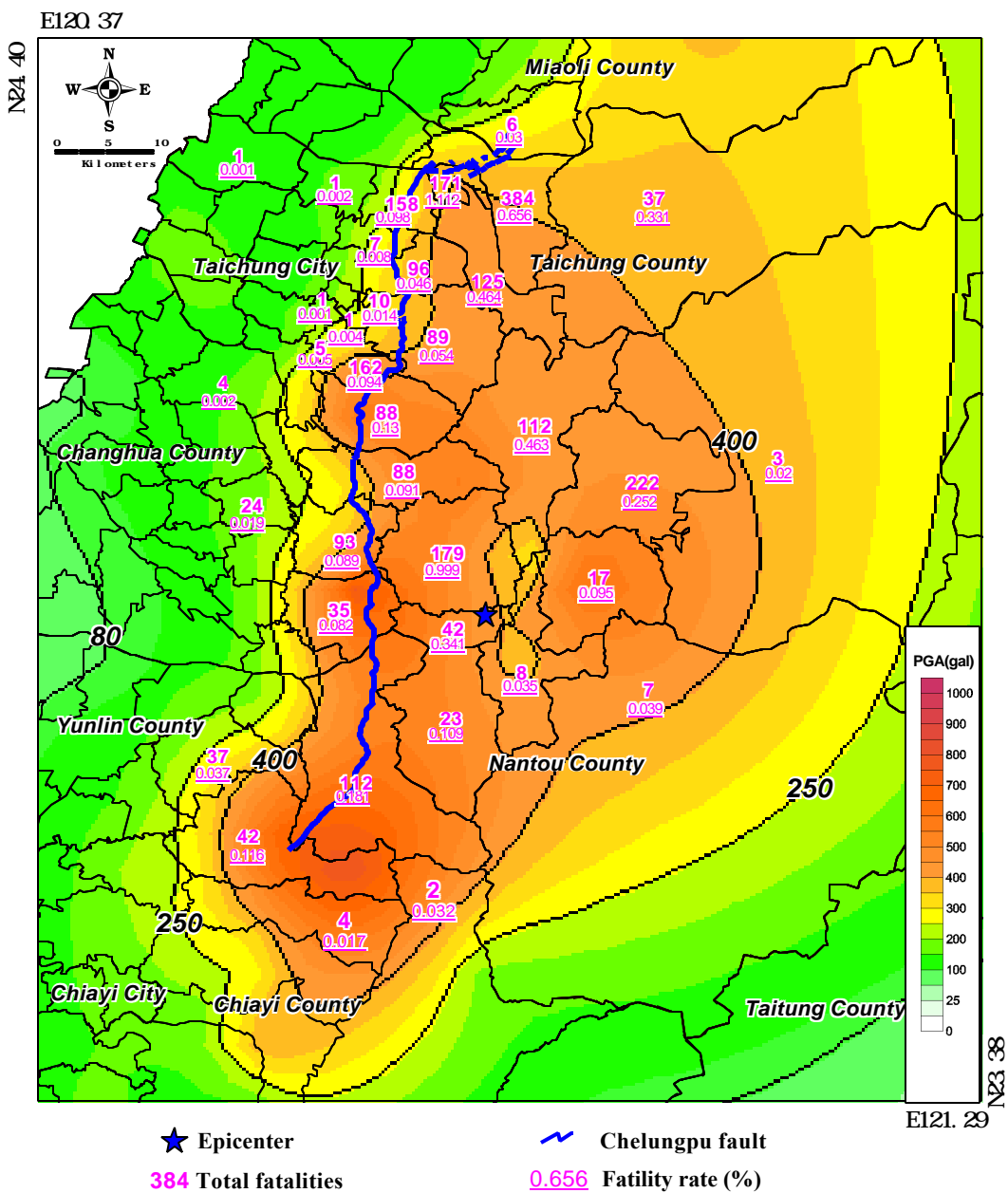
Figure.10 The total fatality and fatality rate (%) of each township. The thick dark curves are contours of horizontal peak ground acceleration in gals in central Taiwan due to the Chi-Chi, Taiwan Earthquake of September 21,1999.
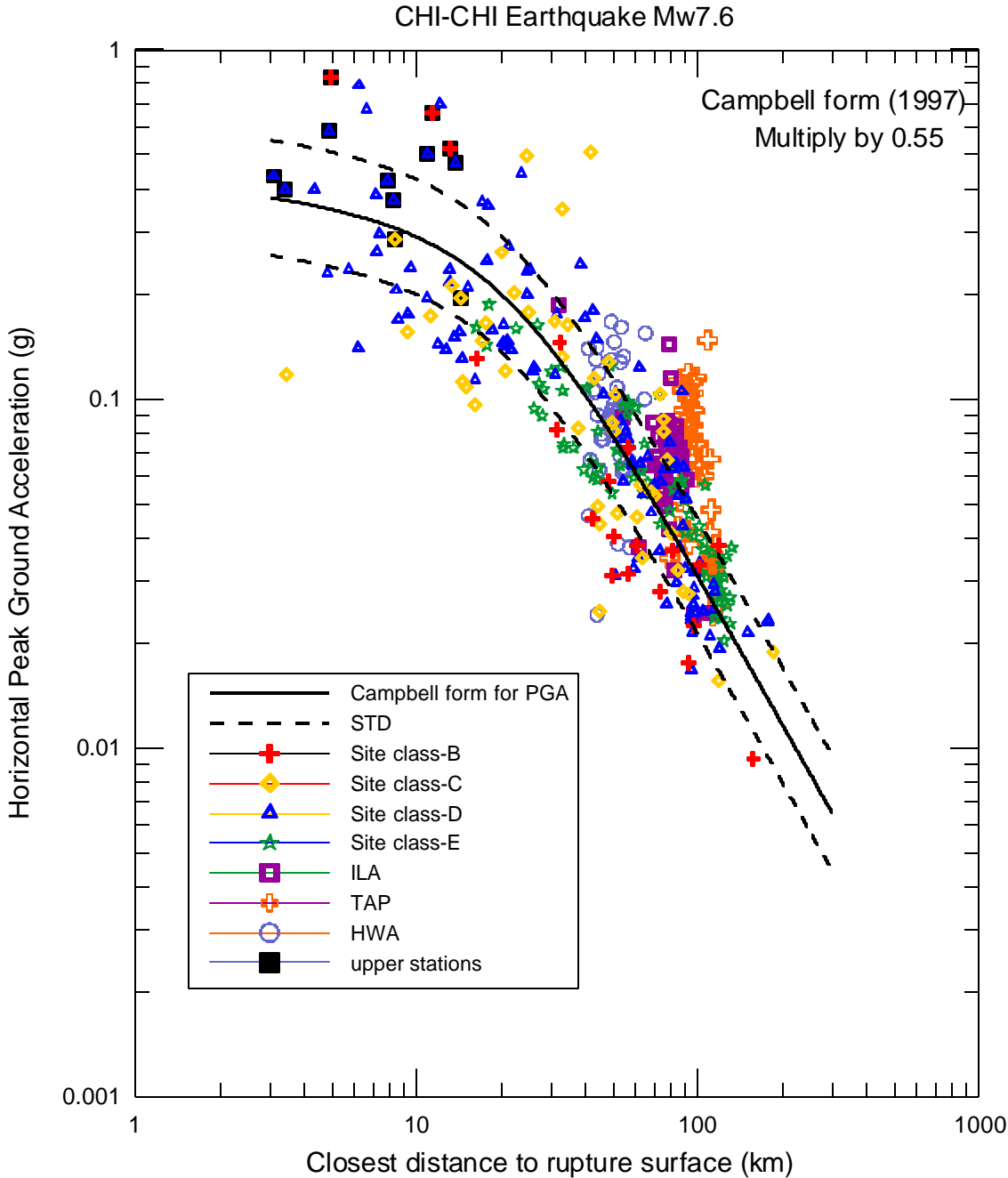
Figure 11. Attenuation of horizontal peak ground acceleration from the Chi-Chi earthquake.
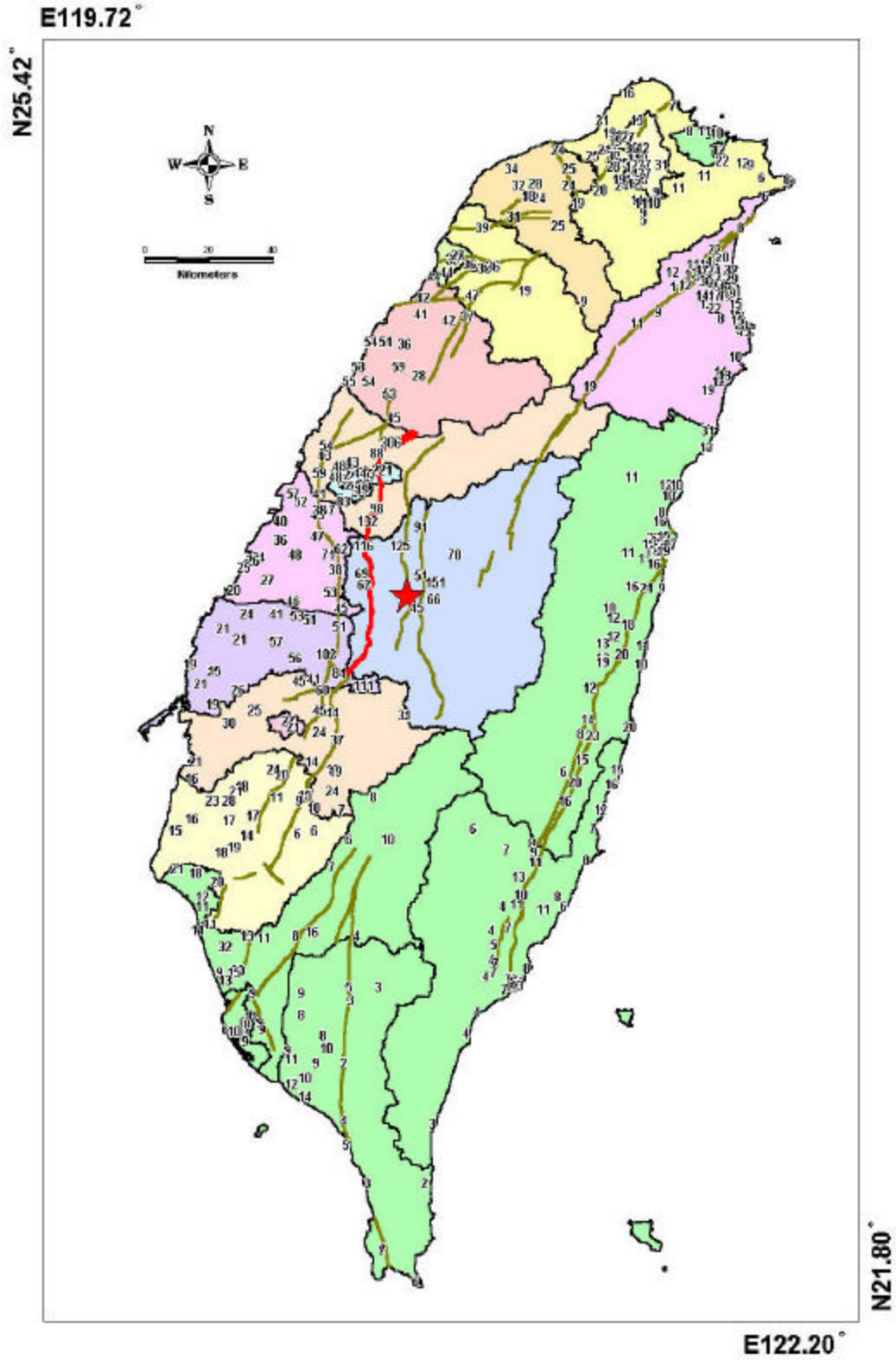
Figure 12. Distribution of integrated horizontal peak ground velocity (in cm/sec) from the Chi-Chi earthquake.
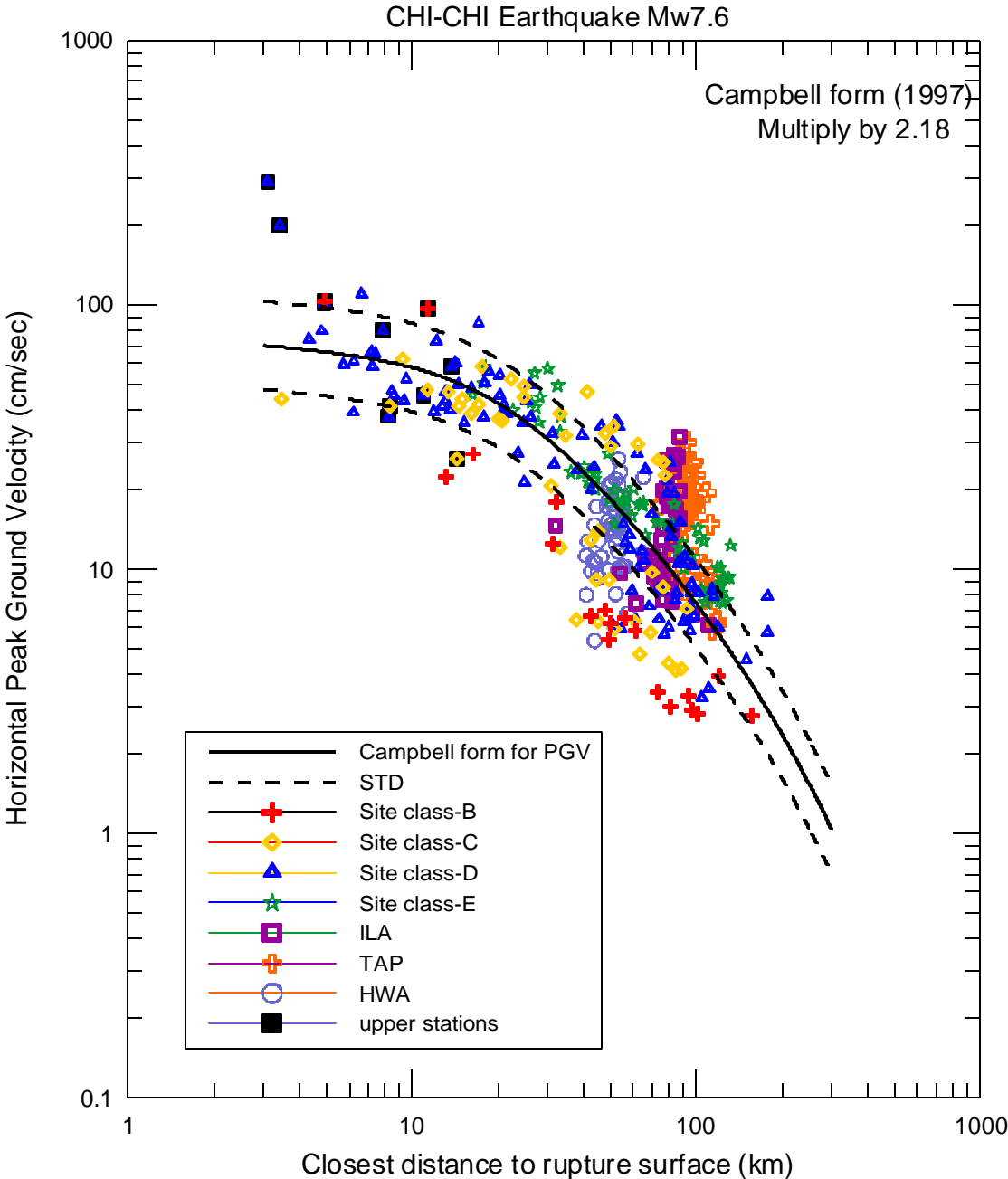
Figure 13. Attenuation of horizontal peak ground velocity from the Chi-Chi earthquake.
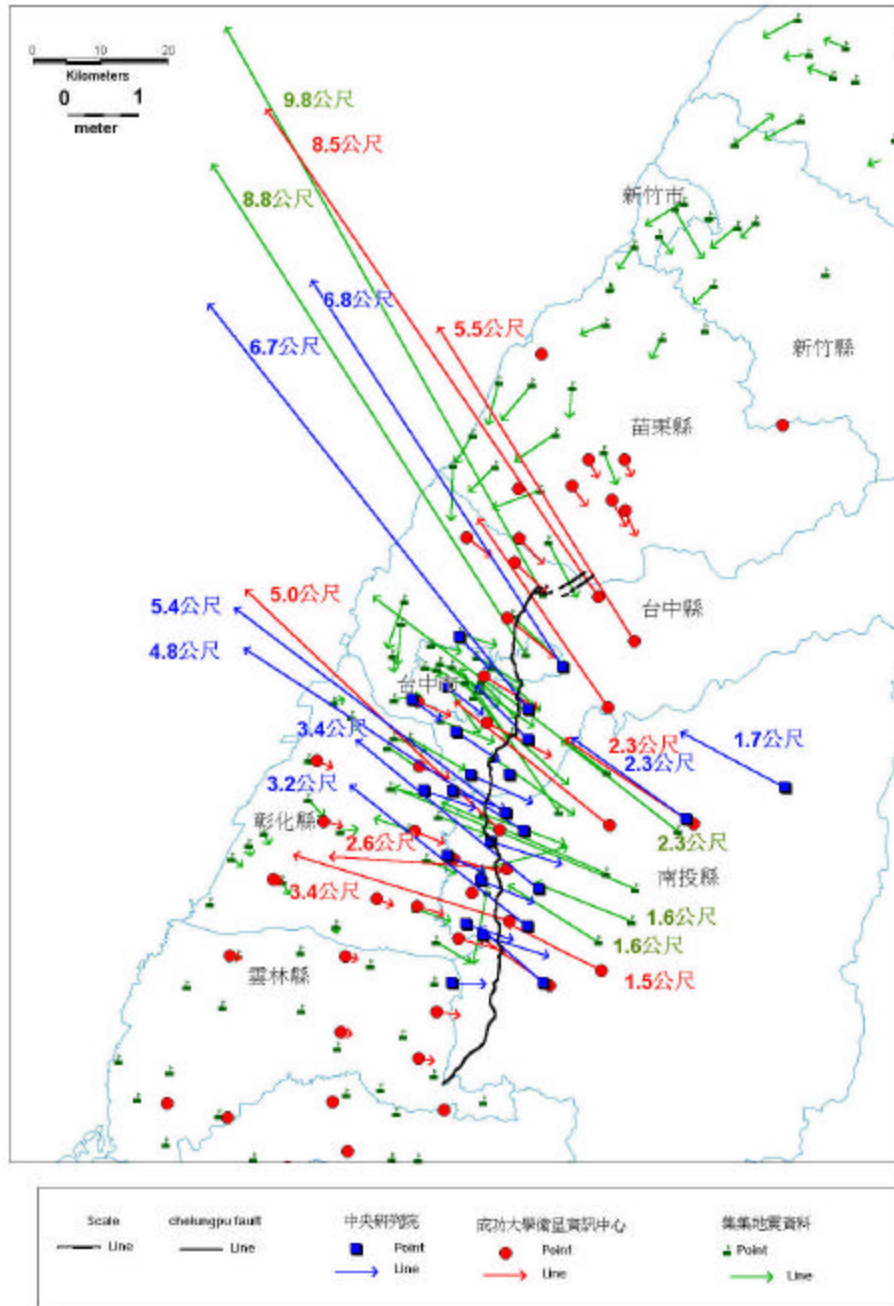
Figure 14. Distribution of integrated permanent horizontal ground displacement vectors from the Chi-Chi earthquake (in green). Also shown are he ground displacements from GPS measurements (in blue and red).
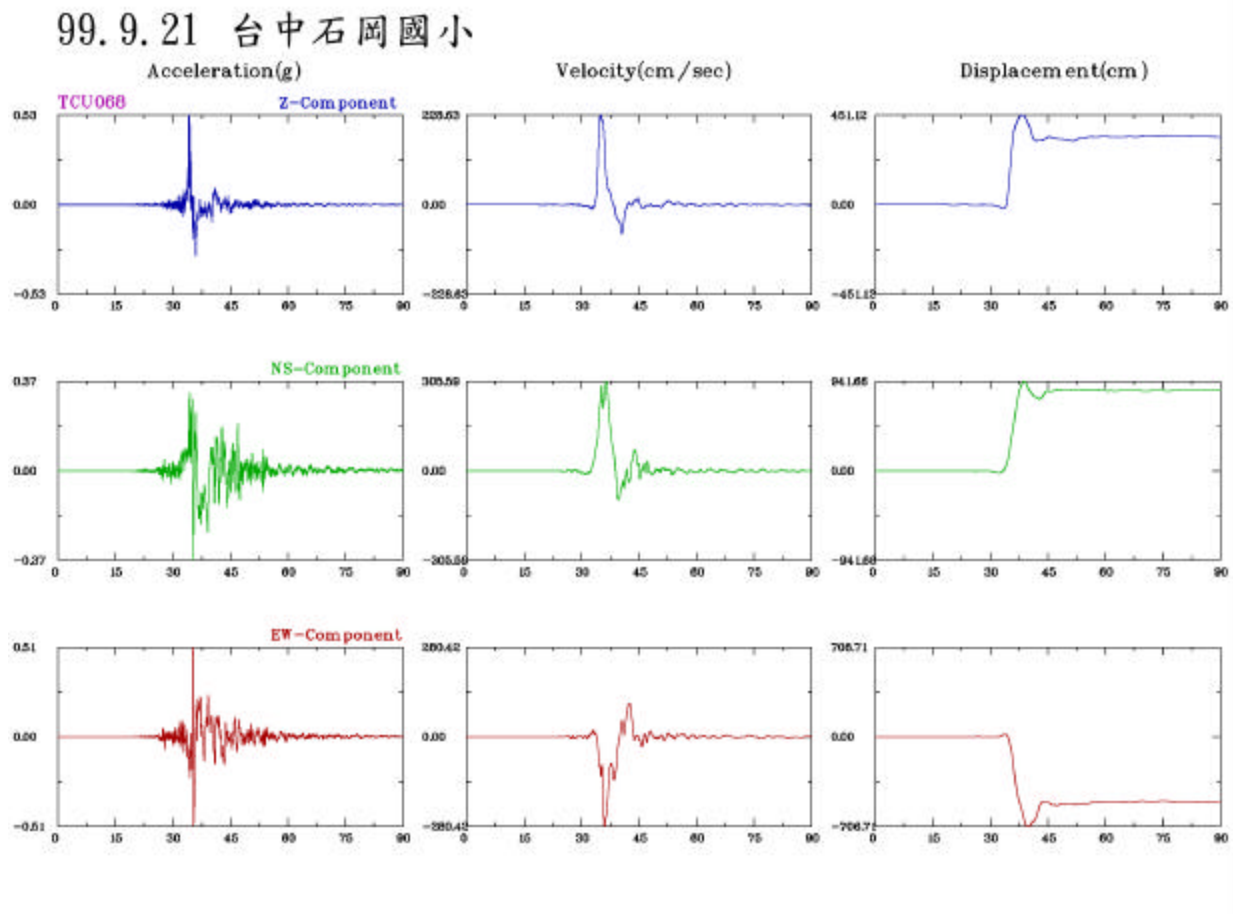
Figure 15. The recorded acceleration, integrated velocity and displacement waveforms at station TCU068 from the Chi-Chi earthquake.
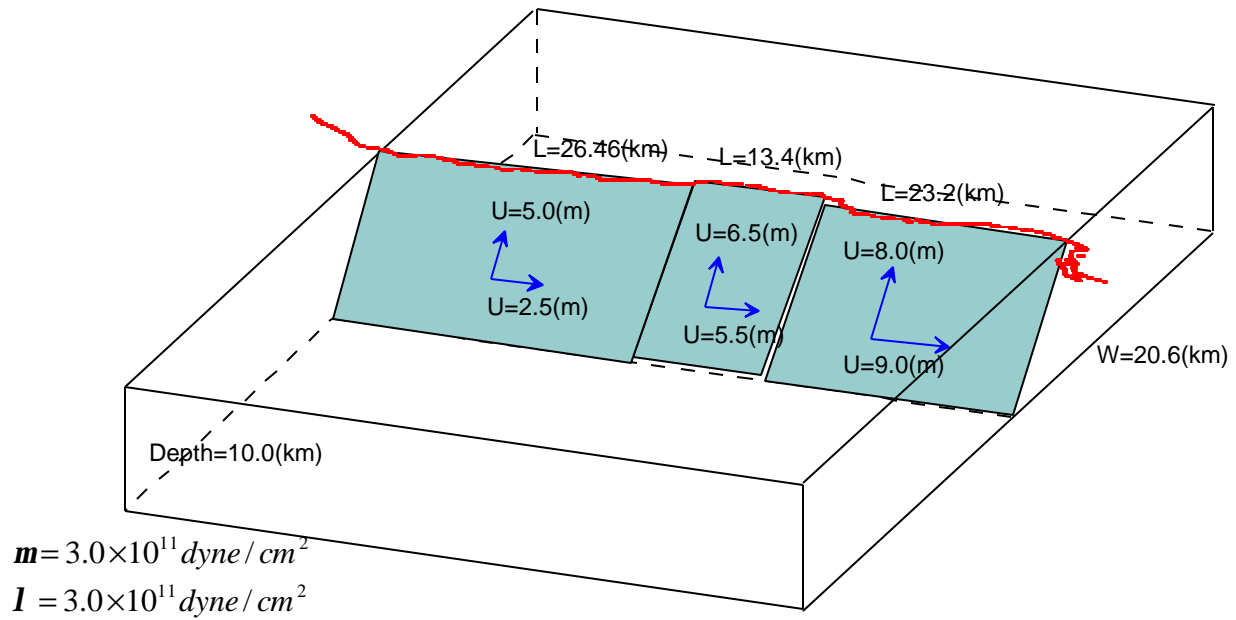
Figure 16. The first-order estimation of the dip-slip and strike-slip displacements in the southern, central and northern segments of the Chelungpu fault.
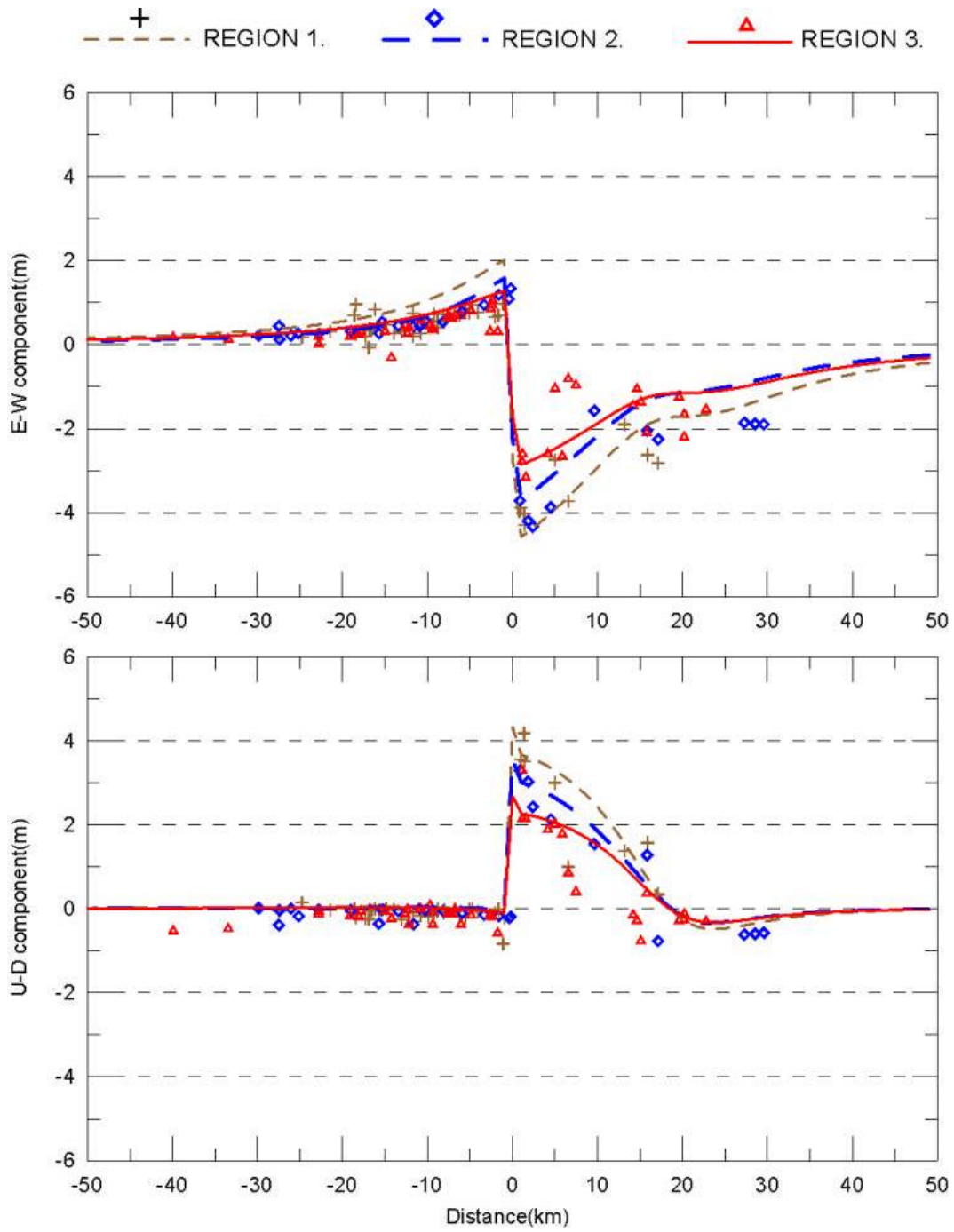
Figure 17. The observed and calculated vertical displacements across the southern, central and northern segments of the fault.
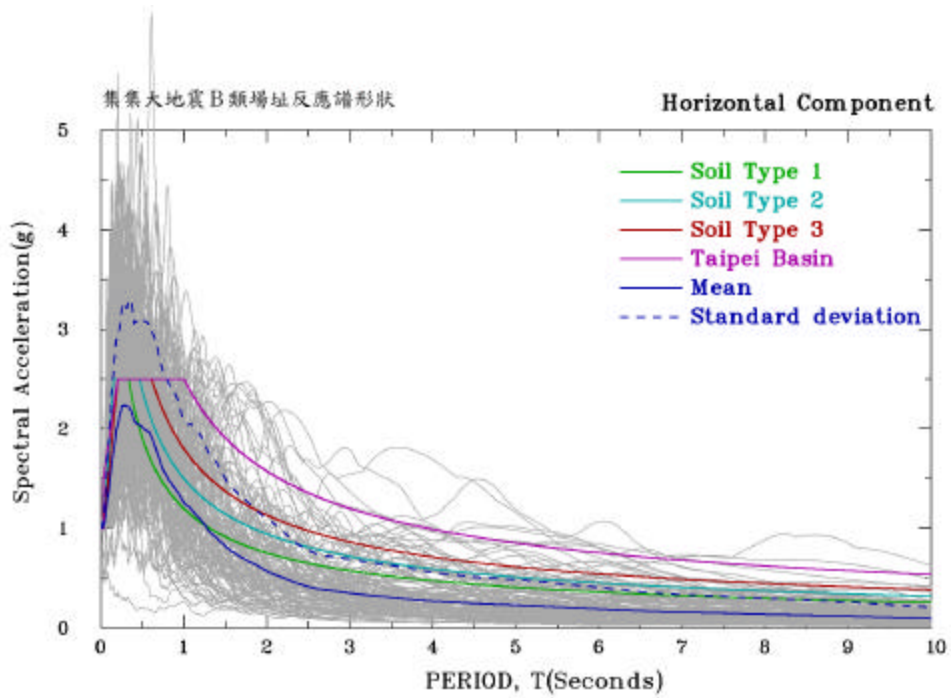
Figure 18. Comparison of the normalized 5% damped acceleration response spectra from Class B sites with the modified Type 1, 2, 3 and Taipei Basin seismic design spectra.
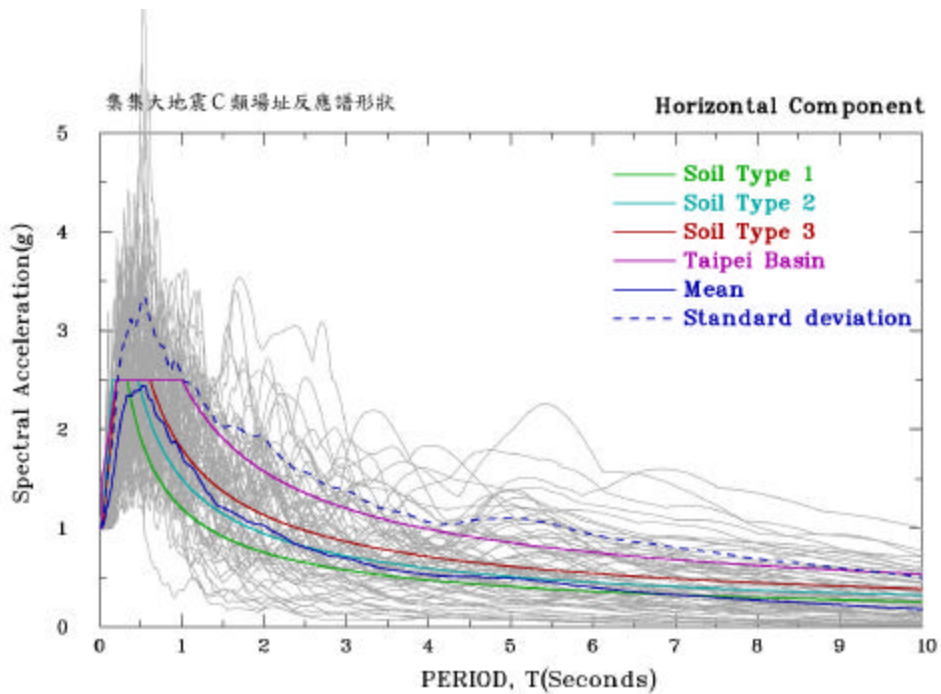
Figure 19. Comparison of the normalized 5% damped acceleration response spectra from Class C sites with the modified Type 1, 2, 3 and Taipei Basin seismic design spectra.
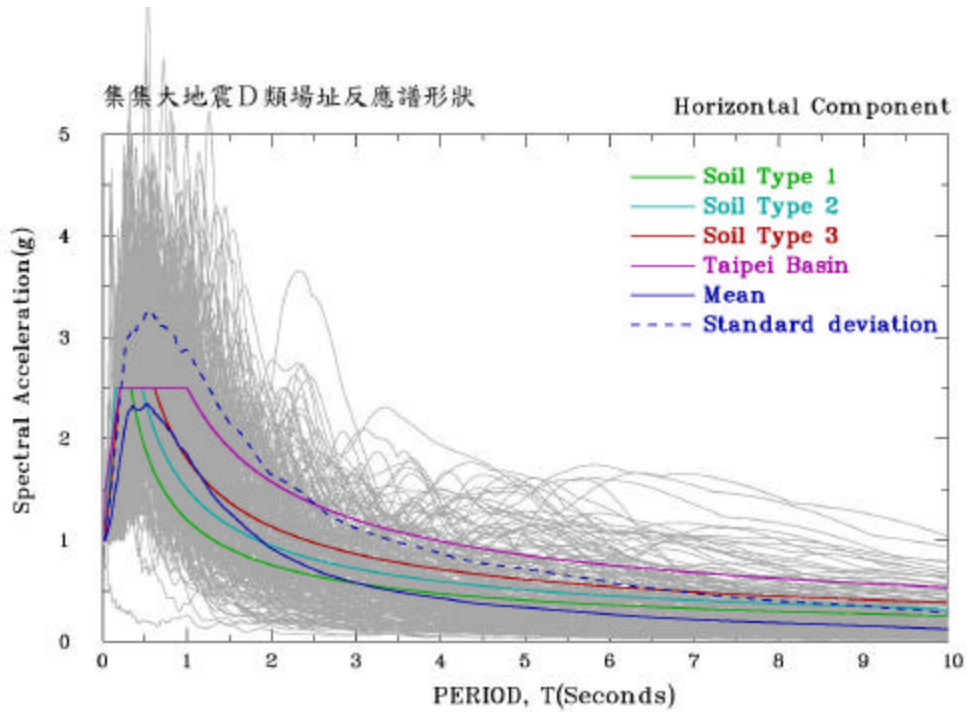
Figure 20. Comparison of the normalized 5% damped acceleration response spectra from Class D sites with the modified Type 1, 2, 3 and Taipei Basin seismic design spectra.
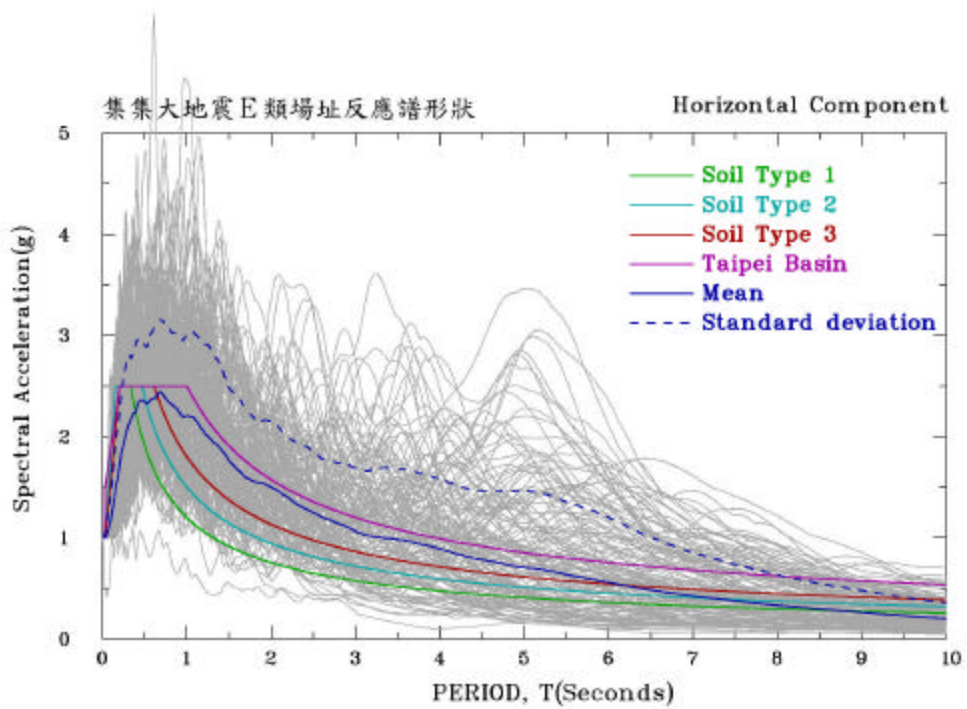
Figure 21. Comparison of the normalized 5% damped acceleration response spectra from Class E sites with the modified Type 1, 2, 3 and Taipei Basin seismic design spectra.
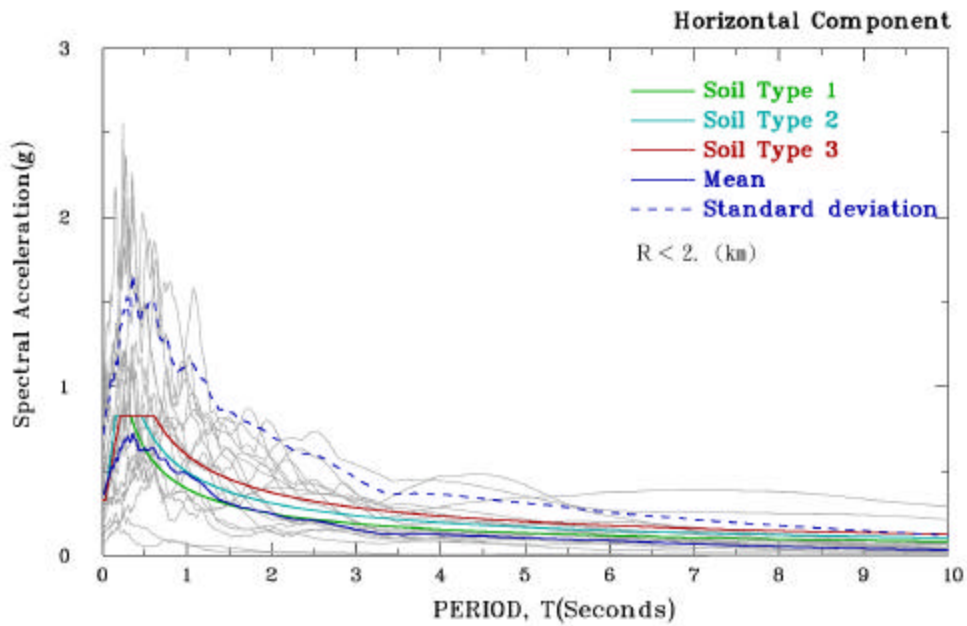
Figure 22. Comparison of 5% damped response acceleration spectra from the recording sites within 2 km of the Chehlungpu fault with the modified seismic design spectra anchored at 0.33g.
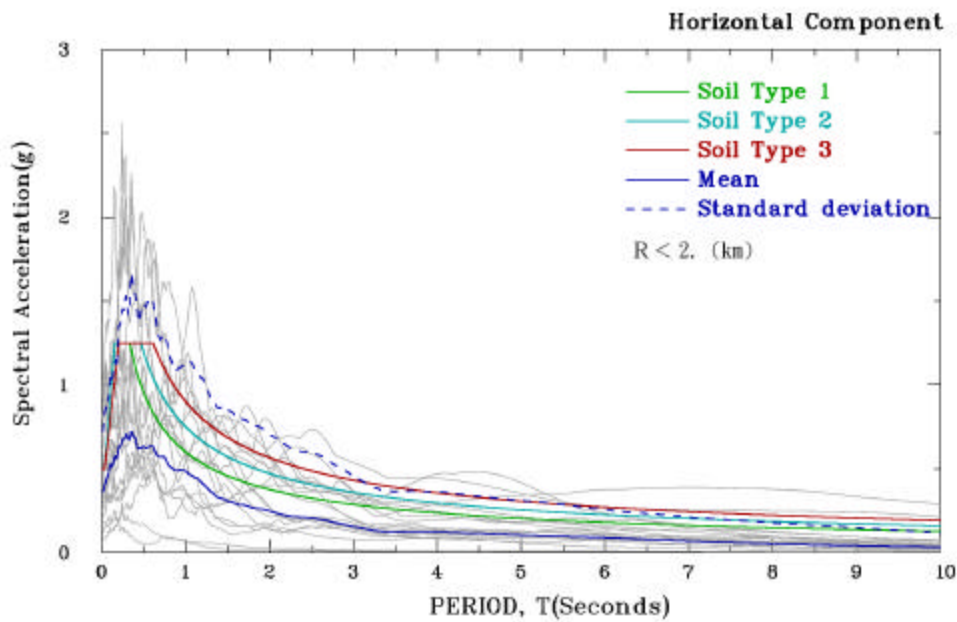
Figure 23. Comparison of 5% damped response acceleration spectra from the recording sites within 2 km of the Chehlungpu fault with the modified seismic design spectra anchored at 0.50g.
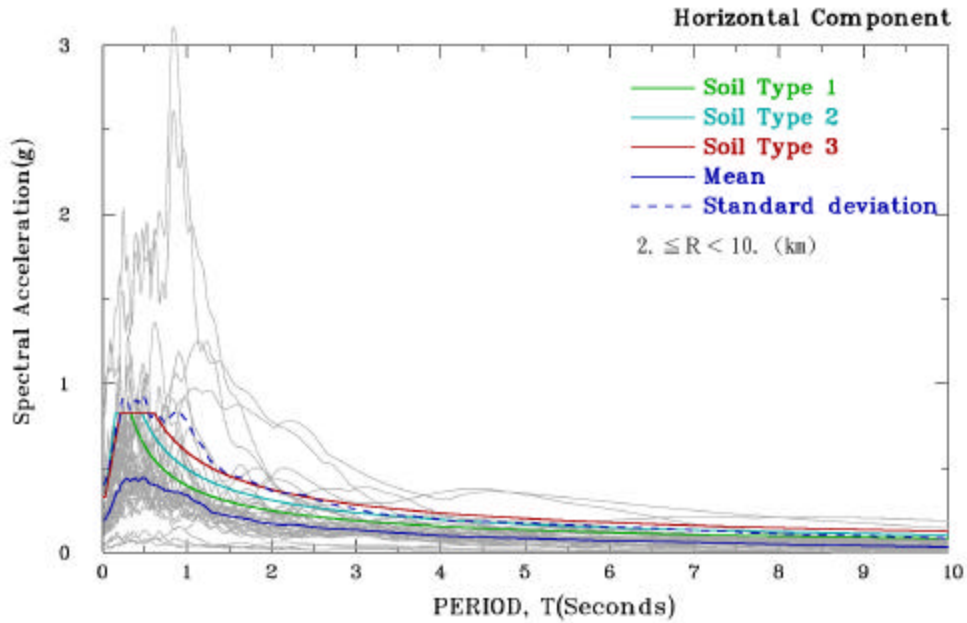
Figure 24. Comparison of 5% damped response acceleration spectra from the recording sites at 2-10 km of the Chehlungpu fault with the modified seismic design spectra anchored at 0.33g.
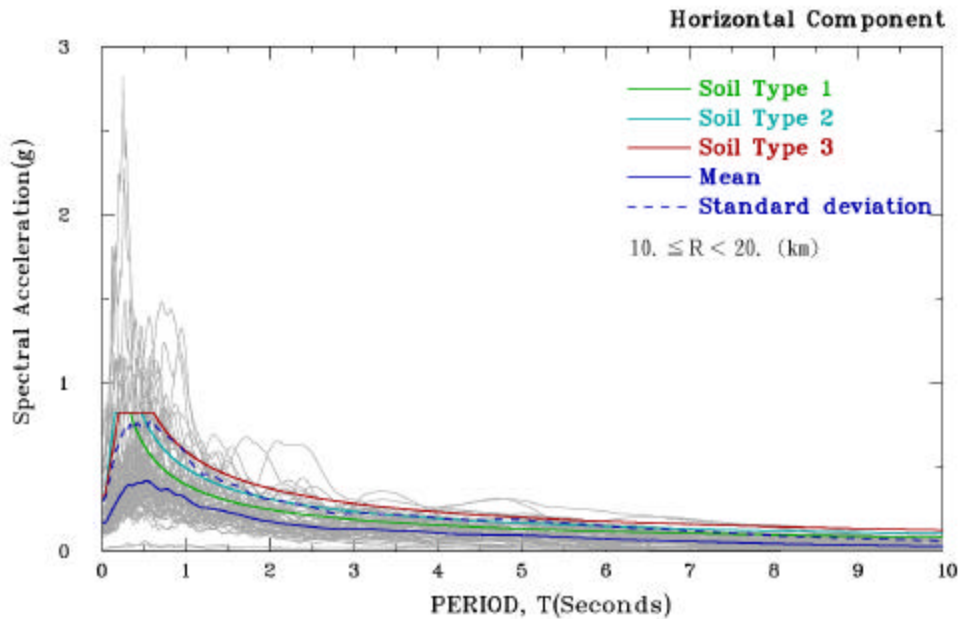
Figure 25. Comparison of 5% damped response acceleration spectra from the recording sites at 10-20 km of the Chehlungpu fault with the modified seismic design spectra anchored at 0.33g

Photo 1.

Photo 2.

Photo 3.

Photo 4.